

Estimating JUNO’s sensitivity to solar neutrino-to-antineutrino conversion and neutrino magnetic moments

C. V. VENTURA¹ AND SAUL J. PANIBRA CHURATA¹

¹Department of General Science, Universidad Continental,
 Av. Los Incas 04002, Arequipa, Perú

ABSTRACT

We investigated JUNO’s sensitivity to a possible conversion of solar neutrinos into antineutrinos via the spin-flavor precession (SFP) mechanism, and assessed the implications for constraining the neutrino-magnetic moment (NMM). Using a sensitivity-based framework appropriate for counting experiments with no prior observations, we derive 90% C.L. ensemble-average sensitivities on the solar antineutrino flux for 1.8–16.8 MeV and 8.0–16.8 MeV. For the entire energy window, the results do not improve the restrictions of other experiments; the relevance occurs in the high-energy window. In this window, we report a flux of $\phi_{\text{lim}} \leq 4.01 \times 10^1 \text{ cm}^{-2} \text{ s}^{-1}$ and a probability of $P_{\nu_e \rightarrow \bar{\nu}_e} \leq 2.07 \times 10^{-5}$, the latter normalized to the ${}^8\text{B}$ flux above threshold, $\Phi_{\text{SSM}}(E > 8 \text{ MeV})$. Assuming transverse solar magnetic fields of $B_{\perp} = 50$ and 100 kG, the corresponding magnetic-moment sensitivities are $\mu_{\nu} \leq 7.27 \times 10^{-11} \mu_B$ and $3.64 \times 10^{-11} \mu_B$ in the high-energy window. These results highlight that JUNO has the potential to achieve sensitivities comparable to the most stringent astrophysical limits; in particular, the high-energy selection (8.0–16.8 MeV) provides a sensitivity that is competitive with current results, while the full-energy window remains primarily limited by near-reactor backgrounds.

Keywords: Solar neutrinos(1511); Neutrino oscillations(1104); Particle astrophysics(96)

1. INTRODUCTION

The investigation of a possible unknown source of antineutrinos to explain observed events unrelated to known-origin sources is crucial for understanding the nature of the neutrino. A hypothetical flux of solar antineutrinos cannot be ruled out as a potential explanation for this unknown source.

Research confirms that neutrinos have mass, a property that leads to the phenomenon of neutrino oscillations, where neutrinos can change flavor as they propagate. This also implies they may possess a small magnetic moment capable of interacting with intense magnetic fields (e.g., Cisneros 1971), such as the solar magnetic field. This interaction induces SFP in Majorana neutrinos, causing a flavor oscillation that converts a neutrino into an antineutrino, $\nu \rightarrow \bar{\nu}$ (Giunti & Studenikin 2009, 2015). Therefore, weak antineutrino fluxes cannot be excluded from the observations.

Over the past decade, neutrino experiments like Borexino (Bellini et al. 2011), KamLAND (Eguchi et al. 2004), and Super-Kamiokande (Fukuda et al. 1998) have significantly contributed to setting upper limits on exotic neutrino signals. Borexino, renowned for its sensitivity to low-energy neutrinos, has placed stringent con-

straints on the solar antineutrino flux and the possible magnitude of the NMM. KamLAND, with its capability to detect antineutrinos from both geophysical and nuclear reactor sources, has also provided valuable detection limits. Meanwhile, Super-Kamiokande, focused on detecting high-energy solar and atmospheric neutrinos, has imposed key restrictions on flavor oscillations and neutrino conversion under exotic mechanisms such as SFP in solar magnetic fields.

Recent studies have further refined constraints on the NMM (μ_{ν}). The most restrictive astrophysical bounds now arise from recent analyses of stellar-cooling in red-giant-branch (TRGB) stars, rather than from earlier globular-cluster estimates. In particular, using *Gaia*-based geometric calibrations of ω Centauri and NGC 4258, Capozzi & Raffelt (2020) derived upper limits of $\mu_{\nu} < 1.2 \times 10^{-12} \mu_B$ and $\mu_{\nu} < 1.5 \times 10^{-12} \mu_B$ (95% C.L.), respectively, representing the most stringent astrophysical constraints to date. Earlier analyses of globular-cluster stars, where excessive neutrino emission would accelerate stellar cooling, had set a weaker limit of $\mu_{\nu} < 3 \times 10^{-12} \mu_B$ (Raffelt & Weiss 1992).

Direct experimental constraints mainly originate from reactor neutrino experiments. The GEMMA experiment at the Kalinin Nuclear Power Plant currently holds the

most stringent direct bound, $\mu_{\bar{\nu}_e} < 3.2 \times 10^{-11} \mu_B$ at 90% confidence level (C.L.), using a high-purity germanium detector positioned 13.9 meters from the reactor core (Beda et al. 2010). Some studies have proposed that incorporating atomic ionization effects in neutrino-electron scattering analyses could enhance this limit, lowering it to $\mu_{\bar{\nu}_e} < 5 \times 10^{-12} \mu_B$ (Wong et al. 2010). However, this claim remains debated, as alternative theoretical evaluations suggest that atomic effects do not significantly influence the neutrino-electron cross-section within the relevant energy range (Voloshin 2010).

Meanwhile, Borexino has set an independent constraint on the effective NMM by analyzing the recoil-electron spectrum from solar neutrinos, yielding $\mu_\nu < 5.4 \times 10^{-11} \mu_B$ at 90% C.L. (Bellini et al. 2011). Additionally, cosmological constraints from Big Bang Nucleosynthesis (BBN) and the Cosmic Microwave Background (CMB) impose a competitive limit, excluding values above $\mu_\nu < 1.6 \times 10^{-11} \mu_B$ (Carenza et al. 2024). Cosmological observations of the effective number of relativistic species (N_{eff}) from BBN and the CMB disfavor Dirac, flavor-universal, diagonal NMM exceeding $2.7 \times 10^{-12} \mu_B$, yielding constraints that surpass current XENONnT/LZ limits and are comparable to those from stellar-cooling analyses (Li & Xu 2023).

In massive stars, nonzero NMM at the $(2\text{--}4) \times 10^{-11} \mu_B$ level can qualitatively alter late burning stages and mass thresholds, even enabling a thermonuclear CO (carbon-oxygen) explosion within a massive star (Type I.7) scenario (Heger et al. 2009). Future developments in reactor neutrino experiments and next-generation cosmological surveys are expected to refine these constraints.

2. THE JUNO EXPERIMENT AND DETECTOR CHARACTERISTICS

The Jiangmen Underground Neutrino Observatory (JUNO) is a large-scale neutrino experiment currently under construction in China, designed primarily to determine the neutrino mass hierarchy and measure oscillation parameters with unprecedented precision. The central detector consists of a spherical liquid scintillator target with a diameter of 35.4 meters, containing 20 kton of ultra-pure liquid scintillator, making it the largest detector of its kind ever built. Surrounding the scintillator, an array of 17,612 20-inch photomultiplier tubes (PMTs) and 25,600 3-inch PMTs provides an optical coverage exceeding 75%, enabling an exceptional energy resolution of $\sim 3\%$ at 1 MeV, crucial for distinguishing the oscillation patterns of reactor neutrinos at a baseline of 53 km. The detector is located ~ 700 meters underground to shield against cosmic ray backgrounds,

significantly enhancing its sensitivity to low-energy neutrino interactions (see, An et al. 2016; Stock 2024).

Beyond its primary goal of reactor neutrino oscillation studies, JUNO will serve as a multi-purpose neutrino observatory, capable of detecting solar neutrinos, geoneutrinos, atmospheric neutrinos, and supernova neutrinos. Thanks to its large volume and the high purity of the liquid scintillator, JUNO will be able to detect Boron-8 solar neutrinos with unprecedented precision, allowing the search for potential signals of solar neutrino-to-antineutrino conversion induced by SFP in solar magnetic fields. Furthermore, the detector’s external veto system, consisting of a water Cherenkov muon detector and an array of plastic scintillators, will help suppress cosmic muon backgrounds, further improving its ability to study neutrino physics and probe physics beyond the Standard Model (see, An et al. 2016; Stock 2024, for more details).

3. FRAMEWORK

3.1. Sensitivity prescription

In a counting experiment where data have not yet been collected, the appropriate figure of merit is the *median upper limit* (or sensitivity), rather than the “maximum allowed signal” S_{lim} corresponding to a particular outcome, which is only relevant once measurements are available.

For $b \lesssim 15$ we use the exact Feldman & Cousins (1998, Table XII) (FC) median limits, whereas for $b \gtrsim 16$ we adopt the one-sided Gaussian approximation,

$$\mu_{\text{UL}}^{90} = 1.28\sqrt{b}, \quad (1)$$

as recommended by the Particle Data Group (2024). This reproduces the FC construction with sub-percent accuracy once $b \gtrsim 16$.

This background dependent approach ensures correct coverage for all b values while avoiding the computational cost of generating extended Feldman-Cousins confidence belts for the $\mathcal{O}(10^3)$ background events expected in the high-threshold analysis window.

The resulting sensitivities—summarized in Table 1 for the two prompt-energy ranges (1.8–16.8 MeV and 8–16.8 MeV)—are then translated into limits on the solar $\bar{\nu}_e$ flux, the spin-flavor conversion probability $P_{\nu_e \rightarrow \bar{\nu}_e}$, and the NMM (μ_ν), using the corresponding energy-averaged inverse beta decay cross sections, $\sigma_A = 3.40 \times 10^{-42} \text{ cm}^2$ and $\sigma_B = 6.64 \times 10^{-42} \text{ cm}^2$.

3.2. Upper Flux Limit and Conversion Probability

The upper limit on the solar antineutrino flux (Bellini et al. 2011), ϕ_{lim} , can be determined according to:

$$\phi_{\text{lim}} = \frac{\mu_{\text{UL}}^{90}}{\sigma T n_p \epsilon} \quad [\text{cm}^{-2} \text{s}^{-1}], \quad (2)$$

where μ_{UL}^{90} is the sensitivity, representing the number of events not associated with any known source. The quantity $\bar{\sigma}$ denotes the *effective inverse beta decay* (IBD) cross section, averaged over the prompt-energy range of interest and weighted by the ${}^8\text{B}$ solar neutrino spectrum.

We obtain the flux-averaged IBD cross section in each window by weighting the energy-dependent cross section with the ${}^8\text{B}$ spectral shape from Bahcall et al. (1996) and averaging over the window limits (1.8–16.8 MeV and 8.0–16.8 MeV). The result reflects the relative contribution of each neutrino energy to the event yield in that window; efficiencies are taken as constant, so they factor out of the average.

The exposure time is $T = 1.5768 \times 10^8$ s (corresponding to five years of continuous data-taking), the number of free proton targets is $n_p = 1.44 \times 10^{33}$ (Abraho et al. 2015), and the overall detection efficiency is taken to be $\epsilon \approx 1$.

The IBD threshold at $E_\nu \simeq 1.80$ MeV (hereafter 1.8 MeV) marks the minimum neutrino energy for the reaction $\bar{\nu}_e + p \rightarrow e^+ + n$, which is the primary detection channel in large liquid-scintillator detectors. For our selections, the window-averaged IBD cross sections are $\bar{\sigma} = 3.40 \times 10^{-42}$ cm 2 in the 1.8–16.8 MeV window and $\bar{\sigma} = 6.64 \times 10^{-42}$ cm 2 in the 8.0–16.8 MeV window, obtained using the Strumia & Vissani prescription folded over the analysis windows. Reactor $\bar{\nu}_e$ spectra are largely confined below 8 MeV and fall steeply above this energy; nevertheless, at JUNO baselines and reactor powers, the residual reactor contribution above 8 MeV is subdominant but non-negligible relative to cosmogenic and atmospheric backgrounds, and is therefore included explicitly in our background model (see Table 1).

3.3. Conversion Probabilities and Magnetic Moments

The probability of converting a neutrino into an antineutrino, $P_{\nu \rightarrow \bar{\nu}}$ (see Ahmedov & Pulido 2003; Barger et al. 2002, for more detail), can be written as the ratio of the flux limit ϕ_{lim} to the solar neutrino flux predicted by the Standard Solar Model (SSM), here $\Phi_{\text{SSM}} = 5.88 \times 10^6$ cm $^{-2}$ s $^{-1}$ refers to the *full* ${}^8\text{B}$ spectrum (Serenelli 2010):

$$P_{\nu \rightarrow \bar{\nu}} = \frac{\phi_{\text{lim}}}{\Phi_{\text{SSM}}}. \quad (3)$$

For the high-energy window (8.0–16.8 MeV), only a subset of the ${}^8\text{B}$ spectrum lies above threshold. Accordingly, we evaluate the conversion probability using the SSM flux integrated above the analysis threshold, $\Phi_{\text{SSM}}(E > E_{\text{th}})$. With the spectral shape from Bahcall et al. normalized to the Serenelli SSM flux, this gives $\Phi_{\text{SSM}}(E > 8.0 \text{ MeV}) = 1.94 \times 10^6$ cm $^{-2}$ s $^{-1}$ for the

high-energy selection, while for the full window we use $\Phi_{\text{SSM}}(E > 1.8 \text{ MeV}) = 5.74 \times 10^6$ cm $^{-2}$ s $^{-1}$. Using the window-appropriate $\Phi_{\text{SSM}}(E > E_{\text{th}})$ prevents an artificial inflation of the inferred sensitivity at high threshold and is reflected in Table 1.

The probability of solar neutrino conversion into antineutrinos in the Large Mixed Angle (LMA) scenario is given by Ahmedov & Pulido (2003),

$$P(\nu \rightarrow \bar{\nu}) \approx 1.8 \times 10^{-10} \sin^2 2\theta \left(\frac{\mu_{\bar{\nu}}}{10^{-12} \mu_B} \frac{B_\perp(0.05R_\odot)}{10 \text{kG}} \right)^2$$

where $\mu_{\bar{\nu}}$ is the transition NMM and B_\perp is the transverse component of the solar magnetic field in the neutrino production region. The value $0.05R_\odot$ is considered because it corresponds to the region where ${}^8\text{B}$ neutrinos are generated (see, Bahcall et al. 1996; Bahcall & Pinsonneault 2004; Bahcall et al. 1963), which dominate the JUNO detection spectrum in the relevant energy range (8–16 MeV). This equation shows that the conversion of ν_e into $\bar{\nu}_e$ inside the Sun is highly suppressed unless $\mu_{\bar{\nu}} B_\perp$ is significantly large. The non-detection of a flux of solar $\bar{\nu}_e$ imposes an upper limit on $P(\nu_e \rightarrow \bar{\nu}_e)$, constraining the NMM to

$$\mu_{\bar{\nu}} \leq 7.4 \times 10^{-7} \left(\frac{P_{\nu \rightarrow \bar{\nu}}}{\sin^2 2\theta_{12}} \right)^{1/2} \frac{\mu_B}{B_\perp [\text{kG}]} \quad (4)$$

which represents one of the most stringent constraints on $\mu_{\bar{\nu}}$ obtained to date. In this equation, $\sin^2 2\theta_{12} = 0.86$ is the neutrino mixing parameter (Gando et al. 2011; Barger et al. 2002; Aliani et al. 2003; de Holanda & Smirnov 2002).

The conversion of solar neutrinos into antineutrinos via SFP critically depends on the transverse magnetic field in the solar interior.

The NMM is a hypothetical property that would allow neutrinos to interact with magnetic fields (Giunti & Studenikin 2009). In the Standard Model, the Dirac NMM is predicted to be extremely small, on the order of $10^{-19} \mu_B$ (Bohr magneton), making it undetectable by current experimental means (Lindner et al. 2017). However, in theories beyond the Standard Model, such as Majorana neutrino models or supersymmetry, imposing a limit on the NMM could be sufficiently feasible in the JUNO experiment.

4. ANALYSIS AND RESULTS

In JUNO, we do not measure the NMM directly. Instead, we derive the ensemble-average 90 % C.L. upper limit on the signal, μ_{UL}^{90} , and convert it into a sensitivity on the $\bar{\nu}_e$ flux. Dividing this flux limit by the SSM ${}^8\text{B}$ prediction yields the conversion probability $P_{\nu_e \rightarrow \bar{\nu}_e}$;

Table 1. 90% C.L. sensitivities (ensemble-average upper limits, $\langle \mu_{\text{UL}}^{90} \rangle$) for each background category and for the total background in the two E_ν windows for JUNO (20 kt, 5 yr, $\epsilon = 1$). Quoted b are the expected event counts; limits use the one-sided Gaussian approximation $\mu_{\text{UL}}^{90} = 1.28\sqrt{b}$ for $b > 0$ and the Feldman–Cousins sensitivity $\mu_{\text{UL}}^{90} = 2.44$ for $b = 0$. Flux limits are $\Phi_{\text{lim}} = \mu_{\text{UL}}^{90}/(\bar{\sigma} T n_p)$ with $\bar{\sigma}_A T n_p = 0.772$ for 1.8–16.8 MeV and $\bar{\sigma}_B T n_p = 1.506$ for 8–16.8 MeV. Probability limits are $P_{\nu_e \rightarrow \bar{\nu}_e} = \Phi_{\text{lim}}/\Phi_{\text{SSM}}(E > E_{\text{th}})$ with $\Phi_{\text{SSM}}(E > 1.8 \text{ MeV}) = 5.74 \times 10^6$ and $\Phi_{\text{SSM}}(E > 8.0 \text{ MeV}) = 1.94 \times 10^6 \text{ cm}^{-2}\text{s}^{-1}$. Note: “Far reactors” denotes regional cores (Daya Bay, Huizhou), while “World reactors” denotes the rest-of-world contribution; the two are disjoint.

Energy window: 1.8–16.8 MeV ($\bar{\sigma}_A T n_p = 0.772$)				
Background	b (evt)	μ_{UL}^{90} (evt)	$\Phi_{\text{lim}} [\text{cm}^{-2}\text{s}^{-1}]$	$P_{\nu_e \rightarrow \bar{\nu}_e}$
Near reactors	98671	402.1	5.21×10^2	9.07×10^{-5}
Far reactors	11205	135.5	1.76×10^2	3.07×10^{-5}
Geoneutrinos	837	37.0	4.80×10^1	8.36×10^{-6}
World reactors	1756	53.6	6.95×10^1	1.21×10^{-5}
Accidentals	798	36.2	4.68×10^1	8.15×10^{-6}
$^9\text{Li}/^8\text{He}$	2143	59.3	7.68×10^1	1.34×10^{-5}
NC atmospheric	247	20.1	2.61×10^1	4.55×10^{-6}
Fast neutrons	247	20.1	2.61×10^1	4.55×10^{-6}
$^{13}\text{C}(\alpha, n)$	91	12.2	1.58×10^1	2.75×10^{-6}
Total A	115 995	435.9	5.65×10^2	9.84×10^{-5}
Energy window: 8–16.8 MeV ($\bar{\sigma}_B T n_p = 1.506$)				
Background	b (evt)	μ_{UL}^{90} (evt)	$\Phi_{\text{lim}} [\text{cm}^{-2}\text{s}^{-1}]$	$P_{\nu_e \rightarrow \bar{\nu}_e}$
Near reactors	712	34.15	2.27×10^1	1.17×10^{-5}
Far reactors	52	9.23	6.13	3.16×10^{-6}
$^9\text{Li}/^8\text{He}$	1294	46.04	3.06×10^1	1.58×10^{-5}
Fast neutrons	145	15.41	1.02×10^1	5.26×10^{-6}
NC atmospheric	145	15.41	1.02×10^1	5.26×10^{-6}
World reactors	20	5.72	3.80	1.96×10^{-6}
Geoneutrinos	0	2.44	1.62	8.36×10^{-7}
Accidentals	0	2.44	1.62	8.36×10^{-7}
$^{13}\text{C}(\alpha, n)$	0	2.44	1.62	8.36×10^{-7}
Total B	2 223	60.35	4.01×10^1	2.07×10^{-5}

inserting P into the SFP relation then gives the corresponding limit on the transition NMM. Any future observation of a magnetic moment substantially larger than this bound would imply efficient $\nu_e \rightarrow \bar{\nu}_e$ conversion in strong solar fields and would thus signal physics beyond the Standard Model.

The residual background rates used here are taken from [Abusleme et al. \(2025, Table 3\)](#) of the JUNO mass-ordering study. That work reports post-selection rates (events/day) for seven categories —geoneutrinos, distant reactor $\bar{\nu}_e$, accidentals, $^9\text{Li}/^8\text{He}$ (β -n), fast neutrons, atmospheric NC interactions, and $^{13}\text{C}(\alpha, n)$ —together with their physical origin and spectral shapes. Each category mimics the IBD signature to some extent: some produce genuine $\bar{\nu}_e$ IBD events (reactors, geoneutrinos), while others yield prompt-delayed correlated pairs that are experimentally indistinguishable from IBD ($^9\text{Li}/^8\text{He}$, fast neutrons, NC). Accidentals, although uncorrelated, also enter the IBD window

through random prompt-delay coincidences. Since our goal is to bound a potential solar $\bar{\nu}_e$ signal—which would be detected via IBD—all categories must be included in the expected background b (see, [Abusleme et al. 2025](#), also the discussion on background modelling and uncorrelated bin-to-bin uncertainties).

In addition to these categories, we explicitly include the reactor background from the eight near cores located at $\simeq 52.5$ km (Taishan-1, Taishan-2, and Yangjiang-1..6) as well as the far reactors (e.g., Daya Bay at ~ 215 km and Huizhou at ~ 265 km). These reactor contributions were evaluated with our in-house simulation that computes the expected event yield by integrating the differential rate dN/dE_ν over the two analysis windows ([Abraho et al. 2015](#)). The code implements three-flavor vacuum oscillations (P_{ee} with PDG parameters), the [Strumia & Vissani](#) IBD cross section, and fission spectra with typical fission fractions (0.59/0.28/0.07/0.06) ([Huber 2011](#); [Mueller et al. 2011](#)).

For each core we use its thermal power and baseline to build the flux, and then fold $\Phi \times \sigma_{\text{IBD}} \times P_{ee}$ over energy, assuming a 20 kt fiducial mass, 5 yr live time, and $\epsilon_{\text{det}} = 1$. This procedure yields per-window reactor+geo counts that, when combined with the remaining categories from [Abusleme et al. \(2025\)](#) (geoneutrinos, accidentals, ${}^9\text{Li}/{}^8\text{He}$, fast- n , ${}^{13}\text{C}(\alpha, n)$, NC), produce updated totals of $b_A = 115\,995$ and $b_B = 2\,223$ events. The corresponding Gaussian one-sided sensitivities are $\mu_{\text{UL}}^{90} = 1.28\sqrt{b}$, i.e., 435.9 and 60.35 events for the low- and high-energy windows, respectively. We adopt the JUNO *normal mass-ordering* per-category rate uncertainties to build the window-level rate systematic $\delta b/b$ and propagate them, together with 1.6% detector-scale systematics and the 11% ${}^8\text{B}$ flux uncertainty, into the error budget reported in Table 3. Inverse-beta-decay events from power reactors are explicitly included, as they dominate the background for a solar $\bar{\nu}_e$ signal at JUNO; see Table 1 for representative reactor IBD rates. Unlike Borexino, where large reactor standoff suppresses this contribution, JUNO’s proximity to multiple cores renders the reactor background the leading component in the analysis windows.

From these rates we compute the expected counts over 5 yr and derive the ensemble-average 90% C.L. upper limit μ_{UL} . For $b \leq 15$ we use the exact [Feldman & Cousins \(1998\)](#) construction; for $b \gtrsim 16$ we adopt the one-sided Gaussian approximation $\mu_{\text{UL}}^{90} = 1.28\sqrt{b}$, whose coverage differs from the exact result by $< 1\%$ once $b \gtrsim 16$ ([Feldman & Cousins 1998](#), Table. XII); see also [Particle Data Group \(2024\)](#). The resulting μ_{UL} values are then converted into limits on the $\bar{\nu}_e$ flux, the conversion probability $P_{\nu_e \rightarrow \bar{\nu}_e}$, and the magnetic moment μ_ν using the window-dependent averaged IBD cross sections (Sec. 3.3).

We reconstructed the residual background spectra ¹ by digitizing Fig. 3 of *Potential to identify neutrino mass ordering with reactor antineutrinos at JUNO* (JUNO-NMO) ([Abusleme et al. 2025](#)), interpolating the shapes over 15 MeV, and extending them above 5 MeV with an exponential tail whose slope is fixed by the local log-slope at 5 MeV. The tail has no tunable parameters: its decay constant is set by the measured log-slope at 5 MeV, and we enforce physically motivated endpoints (e.g., geoneutrinos stop at ~ 3.3 MeV, ${}^{13}\text{C}(\alpha, n)$ at $\sim 7\text{--}7.5$ MeV). Each category is normalized once—either to the JUNO-NMO post-selection rate in 0.8–12.0 MeV (Table 3) or to a validated 1–5 MeV integral—

avoiding double anchoring. Because reactor IBDs are our background (not signal), we compute the near- and far-reactor contributions with an independent reactor model ([Huber-Mueller et al.](#) spectra, three-flavor oscillations, [Strumia & Vissani](#) σ_{IBD} , baseline/power). Finally, we integrate the normalized spectra over 5 yr in 1.8–16.8 MeV and 8.0–16.8 MeV to obtain b_A and b_B ([Ventura & Panibra 2025](#)). This procedure reproduces the official totals where they apply and adds only the physically warranted high-energy part.

It is important to emphasize that only the total background in each energy window is physically meaningful for these limits: probabilities and fluxes are not additive across categories. Per-category numbers are shown solely for comparison and pedagogical purposes; the reported physics limits are those derived from the total b in each window.

We evaluated the sensitivity to the NMM within the SFP framework using the ensemble-average limits derived in this work. The two energy windows considered are 1.8–16.8 MeV and 8–16.8 MeV.

The corresponding conversion probability sensitivities, which are independent of the solar field, are $P_{\nu_e \rightarrow \bar{\nu}_e} \leq 9.84 \times 10^{-5}$ for the 1.8–16.8 MeV window and $P_{\nu_e \rightarrow \bar{\nu}_e} \leq 2.07 \times 10^{-5}$ for the 8–16.8 MeV window. To quantify the impact of these results, the flux sensitivities for the two ranges are $\phi_{\bar{\nu}_e, \text{lim}} \leq 5.65 \times 10^2 \text{ cm}^{-2} \text{ s}^{-1}$ and $4.01 \times 10^1 \text{ cm}^{-2} \text{ s}^{-1}$, respectively, corresponding to window-level background totals of $b_A = 115\,995$ and $b_B = 2\,223$ (see Table 1). In the full 1.8–16.8 MeV window, near/far reactor $\bar{\nu}_e$ dominate the background and JUNO’s projected probability sensitivity does not surpass the tightest existing results. In contrast, in the 8.0–16.8 MeV window the reactor spectrum is strongly suppressed and, once probabilities are computed using $\Phi_{\text{SSM}}(E > E_{\text{th}})$, JUNO becomes competitive—potentially leading (see Fig. 1 and Table 4).

Beyond the rate-based approach adopted here, a binned spectral analysis in energy would provide a more precise estimate of the sensitivity. Explicitly incorporating spectral information improves signal-to-background discrimination and can lead to tighter limits than those obtained from window-integrated counts.

Theoretical considerations regarding the solar magnetic field structure provide essential context for interpreting these limits. The conversion of solar neutrinos into antineutrinos via the SFP mechanism is strongly governed by the strength and spatial structure of the transverse magnetic field (B_\perp) across different regions of the Sun. Helioseismic studies suggest that in the solar core ($r < 0.2R_\odot$) the magnetic field could reach values up to 7 MG, with a gradual decrease through

¹ The analysis codes used in this work are publicly available at Zenodo: <https://doi.org/10.5281/zenodo.17613794>.

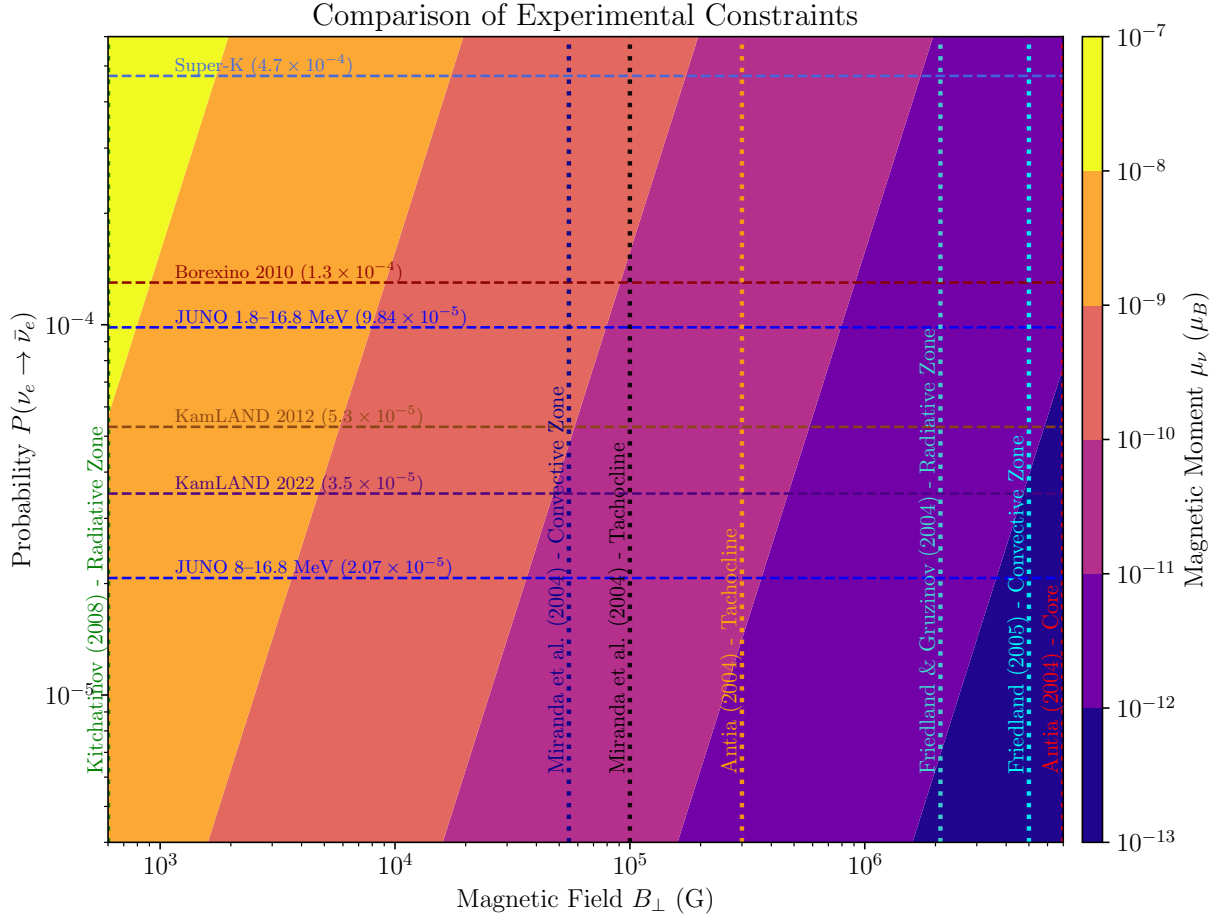


Figure 1. Reference comparison of published upper limits on the conversion probability $P(\nu_e \rightarrow \bar{\nu}_e)$ and their illustrative mapping to magnetic moment sensitivities. **Important:** the experimental (and JUNO projected) limits on P are field-independent; the abscissa B_{\perp} is used here only to visualize how a given probability would translate into μ_{ν} under the scaling $\mu_{\nu} = 7.4 \times 10^{-7} B_{\perp}^{-1} \sqrt{P / \sin^2 2\theta_{12}}$ with $\sin^2 2\theta_{12} = 0.86$. The coloured band encodes the corresponding μ_{ν} (in μ_B) for any pair (P, B_{\perp}) , and should not be interpreted as implying a dependence of P on B_{\perp} . Horizontal dashed lines show the 90% C.L. limits on P from Borexino (2010), KamLAND (2012, 2022), Super-Kamiokande, and the JUNO ensemble-average sensitivities for the two prompt-energy windows (1.8 – 16.8 MeV and 8.0 – 16.8 MeV). Vertical dotted lines mark benchmark field strengths associated with different solar regions (convective zone, tachocline, radiative zone, core). Plotted ranges: $600 \text{ G} \leq B_{\perp} \leq 7 \text{ MG}$ and $5 \times 10^{-6} \leq P \leq 6 \times 10^{-4}$.

the radiative zone (RZ) (see, Antia 2008). In the ${}^8\text{B}$ neutrino production region ($r \approx 0.05R_{\odot}$), where high-energy neutrinos are particularly sensitive to magnetic interactions, the helioseismic model of Antia (2008) estimates a field of approximately 6.56 MG, which is sufficient to allow significant conversion even in the presence of Mikheyev Smirnov Wolfenstein (MSW) suppression. However, stability analyses indicate that toroidal fields in the RZ should not exceed ~ 600 G to avoid inducing instabilities (see, Kitchatinov 2008). When B_{\perp} in this region falls below 600 G, conversion becomes negligible (Bellini et al. 2011).

The lower bound $B_{\perp} \simeq 600$ G reflects the magnetohydrodynamic (MHD) stability threshold for long-lived toroidal fields in the RZ; stronger toroidal fields would

be unstable and thus unlikely to persist over evolutionary timescales.

Beyond the RZ, the tachocline ($r \sim 0.7R_{\odot}$), located at the interface between the radiative and convective zones, hosts magnetic fields estimated between 100 and 300 kG (see, Antia 2008; Friedland 2005). Some studies have considered the possibility of even stronger fields in this region, up to 1 MG, which could enhance the conversion probability (Antia 2008). Importantly, conversion in the tachocline is less affected by MSW suppression than in the core, and its steep magnetic field gradients make it a potentially favorable site for SFP-driven conversion (see, Akhmedov & Pulido 2003, for more detail).

Further outward, the convective zone (CZ) itself is characterized by turbulent and stochastic magnetic

Table 2. Projected 90% C.L. sensitivities of JUNO to $P_{\nu_e \rightarrow \bar{\nu}_e}$ in two windows; $\mu_{\text{UL}}^{90} = 1.28\sqrt{b}$ (or 2.44 if $b \rightarrow 0$). For the high-energy window we use $\Phi_{\text{SSM}}(E > E_{\text{th}})$. Quoted μ_{ν} assume $B_{\perp} = 600$ G and 7 MG (with comparisons made primarily in P , noting $\mu_{\nu} \propto \sqrt{P}/B_{\perp}$).

Energy	$\Phi_{\bar{\nu}_e, \text{lim}}$	$P_{\nu_e \rightarrow \bar{\nu}_e}$	$\mu_{\nu}(600 \text{ G})$	$\mu_{\nu}(7 \text{ MG})$
(MeV)	[$\text{cm}^{-2}\text{s}^{-1}$]	[10^{-5}]	[μ_B]	[μ_B]
1.8–16.8	5.65×10^2	9.84	1.33×10^{-8}	1.13×10^{-12}
8.0–16.8	4.01×10^1	2.07	6.07×10^{-9}	5.18×10^{-13}

fields in the range of 50 to 100 kG (see, [Miranda, O. G. and Rashba, T. I. and Rez, A. I. and Valle, J. W. F. 2004; Miranda et al. 2004; Raffelt & Weiss 1992](#)). Turbulent magnetic field models indicate that if $B_{\perp} < 100$ kG, the conversion probability is negligible, whereas for values approaching 1 MG, the effect could be substantial ([Miranda, O. G. and Rashba, T. I. and Rez, A. I. and Valle, J. W. F. 2004; Miranda et al. 2004](#)). Fluctuations on spatial scales of 100–1000 km match the solar-neutrino oscillation length, enabling resonant conditions for the SFP mechanism ([Miranda, O. G. and Rashba, T. I. and Rez, A. I. and Valle, J. W. F. 2004](#)). Moreover, turbulence induces loss of spin coherence, which can further amplify the conversion probability ([Miranda et al. 2004](#)). These considerations suggest that while a field $B_{\perp} > 1$ MG at $0.05R_{\odot}$ could overcome oscillation suppression in the core, values above 300 kG in the tachocline or sufficiently coherent turbulent fields in the CZ could also support efficient $\nu_e \rightarrow \bar{\nu}_e$ conversion.

Building on this framework, for a transverse field $B_{\perp} = 600$ G we obtain $\mu_{\nu} \leq 1.33 \times 10^{-8} \mu_B$ (1.8–16.8 MeV) and $\mu_{\nu} \leq 6.07 \times 10^{-9} \mu_B$ (8–16.8 MeV). For $B_{\perp} = 7$ MG the limits become $\mu_{\nu} \leq 1.13 \times 10^{-12} \mu_B$ and $\mu_{\nu} \leq 5.18 \times 10^{-13} \mu_B$, respectively (see Table 2). These results follow directly from the field scaling $\mu_{\nu} \propto 1/B_{\perp}$ applied to the probability limits above, and reflect the improved background conditions at higher visible energy threshold.

Within the same setup, the projected sensitivities at the 90% C.L. are as follows.

Full window (1.8–16.8 MeV): the conversion probability satisfies $P_{\nu_e \rightarrow \bar{\nu}_e} \leq 9.84 \times 10^{-5}$, which corresponds to an antineutrino flux bound $\Phi_{\bar{\nu}_e} \leq 5.65 \times 10^2 \text{ cm}^{-2} \text{ s}^{-1}$ (see Table 1). Interpreting this probability in terms of the NMM gives $\mu_{\nu} \leq 1.58 \times 10^{-10} \mu_B$ for $B_{\perp} = 50$ kG and $\mu_{\nu} \leq 7.91 \times 10^{-11} \mu_B$ for $B_{\perp} = 100$ kG (see Table 4).

High-energy window (8–16.8 MeV): the conversion probability satisfies $P_{\nu_e \rightarrow \bar{\nu}_e} \leq 2.07 \times 10^{-5}$, corresponding to $\Phi_{\bar{\nu}_e} \leq 4.01 \times 10^1 \text{ cm}^{-2} \text{ s}^{-1}$ (see Table 1). The associated magnetic-moment limits are $\mu_{\nu} \leq 7.27 \times 10^{-11} \mu_B$

Table 3. Relative uncertainties (%) propagated from background counts to antineutrino flux, conversion probability, and NMM, now including near (8 cores at ~ 52.5 km) and far/world reactor backgrounds. The statistical component is $\sigma_{\text{stat}} = 1/\sqrt{b}$; rate and shape systematics are taken from Tab. 3 of [Abusleme et al. \(2025\)](#). A common detector factor $\delta k/k = 1.6\%$ (0.4% cross section ([Strumia & Vissani 2003](#)), 1% efficiency, 0.3% target protons ([An et al. 2016](#))) is included in $\delta\Phi/\Phi$. The ^8B flux carries an 11% uncertainty ([Vinyoles et al. 2017](#)), which dominates $\delta P/P$ and therefore $\delta\mu/\mu$. Results correspond to a 5-yr exposure; total backgrounds are updated to $b_A = 115,995$ and $b_B = 2,223$, which imply $\mu_{\text{UL}}^{90} = 435.9$ and 60.35 events, respectively, using the 90% C.L. one-sided Gaussian sensitivity $\mu_{\text{UL}}^{90} = 1.28\sqrt{b}$. For probability limits we use $\Phi_{\text{SSM}}(E > 1.8 \text{ MeV}) = 5.74 \times 10^6$ and $\Phi_{\text{SSM}}(E > 8.0 \text{ MeV}) = 1.94 \times 10^6 \text{ cm}^{-2}\text{s}^{-1}$.

Energy window: 1.8–16.8 MeV				
Background	$\delta b/b$	$\delta\Phi/\Phi$	$\delta P/P$	$\delta\mu/\mu$
Near reactors	2.2	1.9	11.2	5.6
Far/world reactors	2.0	1.9	11.2	5.6
Geoneutrinos	30.0	15.1	18.7	9.3
Accidentals	1.0	1.7	11.1	5.6
$^9\text{Li}/^8\text{He}$	20.0	10.1	15.0	7.5
Fast neutrons	100.0	50.0	51.2	25.6
$^{13}\text{C}(\alpha, \text{n})^{16}\text{O}$	50.0	25.1	27.4	13.7
NC atmospheric	50.0	25.1	27.4	13.7
Total A	2.0	1.9	11.2	5.6
Energy window: 8–16.8 MeV				
Background	$\delta b/b$	$\delta\Phi/\Phi$	$\delta P/P$	$\delta\mu/\mu$
$^9\text{Li}/^8\text{He}$	20.0	10.2	15.0	7.5
Fast neutrons	100.0	50.0	51.2	25.6
NC atmospheric	50.0	25.1	27.4	13.7
Total B	11.1	5.9	12.5	6.2

for $B_{\perp} = 50$ kG and $\mu_{\nu} \leq 3.64 \times 10^{-11} \mu_B$ for $B_{\perp} = 100$ kG (see Table 4).

The estimated magnetic moment of solar neutrinos, using a conservative magnetic field and the SFP mechanism, shows values on the order of $\sim 10^{-11} \mu_B$, depending on the magnetic field and conversion probabilities used. Comparing these values with the results obtained from various experiments, several key observations can be made.

A salient outcome of our comparison (Figure 1, Table 4) is the clear window dependence of JUNO’s reach. In the full 1.8–16.8 MeV selection, the sensitivity remains background-limited by power-reactor $\bar{\nu}_e$ (eight near cores at ~ 52.5 km plus the far/world component; see Table 1), and does not surpass the tightest existing results [$P_{\nu_e \rightarrow \bar{\nu}_e} \simeq 9.84 \times 10^{-5}$ for JUNO]. In contrast, in the 8.0–16.8 MeV window the reactor spectrum

is strongly suppressed; adopting the appropriate normalization to the ${}^8\text{B}$ flux above threshold, $\Phi_{\text{SSM}}(E > E_{\text{th}})$ —with $\Phi_{\text{SSM}}(E > 8 \text{ MeV}) = 1.94 \times 10^6 \text{ cm}^{-2} \text{ s}^{-1}$ —JUNO becomes competitive and slightly leading, with a projected $P_{\nu_e \rightarrow \bar{\nu}_e} \simeq 2.07 \times 10^{-5}$ (compared to KamLAND’s $\simeq 3.5 \times 10^{-5}$). This high-energy selection therefore captures JUNO’s comparative advantage for $P_{\nu_e \rightarrow \bar{\nu}_e}$ and, by scaling $\mu_\nu \propto \sqrt{P}/B_\perp$, yields a modest but meaningful tightening of the corresponding NMM sensitivity.

For the KamLAND experiment, an upper limit for the magnetic moment of solar neutrinos was obtained, $\mu_\nu \leq 3.5 \times 10^{-12} \mu_B$ (90% C.L.), based on the observation of the conversion of ${}^8\text{B}$ solar neutrinos to antineutrinos (Gando et al. 2012). This limit is one of the strictest obtained in solar neutrino experiments through this conversion process.

Table 4. Published 90% C.L. limits (no re-scaling of P or ϕ). Magnetic moment values are uniformly rescaled to $B_\perp = 50, 100 \text{ kG}$ for comparisons across experiments; primary comparisons in the text are given in terms of $P_{\nu_e \rightarrow \bar{\nu}}$. Note: $\mu_\nu = \frac{7.4 \times 10^{-7}}{B_\perp [\text{kG}]} \sqrt{P_{\text{lim}} / \sin^2 2\theta_{12}}$ with $\sin^2 2\theta_{12} = 0.86$.

Experiment	Energy threshold (MeV)	P_{lim}	Flux $\phi_{\bar{\nu}}$ [$\text{cm}^{-2} \text{ s}^{-1}$]	B $_\perp = 50 \text{ kG}$		B $_\perp = 100 \text{ kG}$	
				(μ_B)	(μ_B)	(μ_B)	(μ_B)
CTF (Balata et al. 2006)	> 1.8	1.9×10^{-2}	1.1×10^5	2.20×10^{-9}	1.10×10^{-9}		
SNO (Aharmim et al. 2004)	4.0–14.8	8.1×10^{-3}	4.09×10^4	1.44×10^{-9}	7.18×10^{-10}		
Super-Kamiokande (Abe et al. 2022a)	9.3–17.3	4.7×10^{-4}	4.04×10^4	3.46×10^{-10}	1.73×10^{-10}		
KamLAND (2004) (Eguchi et al. 2004)	8.3–14.8	2.8×10^{-4}	1250	2.67×10^{-10}	1.33×10^{-10}		
Borexino (2011; high thr.) (Bellini et al. 2011)	> 7.3	1.7×10^{-4}	990	2.08×10^{-10}	1.04×10^{-10}		
Borexino (2011; combined) (Bellini et al. 2011)	> 1.8	1.3×10^{-4}	760	1.82×10^{-10}	9.10×10^{-11}		
KamLAND (2012) (Gando et al. 2012)	8.3–31.8	5.3×10^{-5}	—	1.16×10^{-10}	5.81×10^{-11}		
KamLAND (2022) (Abe et al. 2022b)	8.3–30.8	3.5×10^{-5}	60	9.44×10^{-11}	4.72×10^{-11}		
JUNO (this work, $b = 115\,995$)	1.8–16.8	9.84×10^{-5}	565	1.58×10^{-10}	7.91×10^{-11}		
JUNO (this work, $b = 2\,223$)	8.0–16.8	2.07×10^{-5}	40.1	7.27×10^{-11}	3.64×10^{-11}		

Figure 1 provides a comparative overview of published limits on the conversion probability $P(\nu_e \rightarrow \bar{\nu}_e)$. The color map encodes the corresponding magnetic-moment limit $\mu_\nu \propto B_\perp^{-1} \sqrt{P}$ for benchmark transverse fields B_\perp , while vertical guide lines mark representative solar-field benchmarks (convective zone, tachocline, radiative zone, core). The plotted ranges are $600 \text{ G} \leq B_\perp \leq 7 \text{ MG}$ and $5 \times 10^{-6} \leq P \leq 6 \times 10^{-4}$. Dashed horizontal lines indicate the 90% C.L. bounds from Super-Kamiokande (4.7×10^{-4}) (Abe et al. 2022a), Borexino (1.3×10^{-4}) (Bellini et al. 2011), and KamLAND ($5.3 \times 10^{-5}, 3.5 \times 10^{-5}$) (Gando et al. 2012; Abe et al. 2022b). Two additional horizontal lines show JUNO’s ensemble-average sensitivities for 1.8–16.8 MeV and 8.0–

In Borexino, a limit for the magnetic moment of solar neutrinos of $\mu_\nu \leq 1.4 \times 10^{-12} \mu_B$ was derived, using experimental data and a conversion probability of $P_{\nu \rightarrow \bar{\nu}} = 1.3 \times 10^{-4}$ (Bellini et al. 2011).

The Super-Kamiokande experiment, for its part, established a limit of $\mu_\nu \leq 3.6 \times 10^{-10} \mu_B$ based on 1496 days of solar neutrino data. This limit was improved to $\mu_\nu \leq 1.1 \times 10^{-10} \mu_B$ when additional restrictions from neutrino oscillation experiments were considered (Abe et al. 2022a).

Finally, the analysis from SNO on solar neutrinos also established a limit on the magnetic moment of $\mu_\nu \leq 1.4 \times 10^{-12} \mu_B$, based on the conversion of ${}^8\text{B}$ solar neutrinos to antineutrinos (Aharmim et al. 2004).

16.8 MeV, at $P \leq 9.84 \times 10^{-5}$ and $P \leq 2.07 \times 10^{-5}$, respectively. While the full-window sensitivity does not surpass the tightest existing limit, the 8.0–16.8 MeV selection lies well below previous results and thus implies stronger μ_ν bounds across the benchmark field range.

Table 3 summarizes the relative uncertainties propagated from the background expectations to the flux, conversion probability, and magnetic-moment sensitivities. For the full window (1.8–16.8 MeV) we obtain $\delta\Phi/\Phi \simeq 1.9\%$, $\delta P/P \simeq 11.2\%$, and $\delta\mu/\mu \simeq 5.6\%$. For the high-energy window (8.0–16.8 MeV) the corresponding values are $\delta\Phi/\Phi \simeq 5.9\%$, $\delta P/P \simeq 12.5\%$, and $\delta\mu/\mu \simeq 6.2\%$. These figures already include the common detector normalization ($\delta k/k = 1.6\%$) with $k = \bar{\sigma} T N_p \varepsilon$ (0.4% IBD

cross section, 1.0% efficiency, 0.3% target protons) and the 11% uncertainty on the solar ${}^8\text{B}$ flux. After these inputs, the residual error budget is dominated by background modeling—geoneutrinos and ${}^9\text{Li}/{}^8\text{He}$ in the full window, and ${}^9\text{Li}/{}^8\text{He}$ plus fast neutrons (with a sub-leading atmospheric-NC component) in the high-energy window.

Total uncertainties are obtained by adding in quadrature uncorrelated rate and statistical contributions across backgrounds. We stress that these fractional errors are independent of the assumed solar field B_{\perp} (which only rescales $\mu_{\nu} \propto 1/B_{\perp}$), and they are a factor 2-3 smaller than the quoted fractional errors in Borexino and KamLAND (Bellini et al. 2011; Gando et al. 2012), underscoring the robustness of JUNO’s sensitivity. To place these results in context, the flux, probabilities, and magnetic moment obtained in this study are compared with previous experimental constraints. In summary, these comparisons, shown in Table 4, highlight the potential of JUNO to refine current limits and contribute substantially to the global understanding of neutrino properties.

5. CONCLUSIONS

We have investigated the possible conversion of solar neutrinos into antineutrinos via SFP and assessed its implications for the NMM. Using a sensitivity-based framework appropriate for counting experiments with no prior observations in this channel, we derived ensemble-average 90% C.L. sensitivities to the solar $\bar{\nu}_e$ flux in two prompt-energy ranges, 1.8–16.8 MeV and 8.0–16.8 MeV.

Our updated background model, summarized in Table 1, shows that antineutrinos from the eight nearest reactors at a baseline of $\simeq 52.5$ km dominate the low-energy region at JUNO, while contributions from distant/world reactors, geoneutrinos, cosmogenics, fast neutrons, ${}^{13}\text{C}(\alpha, n)$, accidentals, and atmospheric NC interactions are also included. Above 8 MeV the reactor spectrum is strongly suppressed, leaving cosmogenic and atmospheric sources as the leading backgrounds; these are explicitly accounted for in the high-energy sensitivity calculation, where probabilities are normalized to the fraction of the ${}^8\text{B}$ flux above threshold, $\Phi_{\text{SSM}}(E > E_{\text{th}})$.

For the full 1.8–16.8 MeV window we obtain $\phi_{\text{lim}} \leq 5.65 \times 10^2 \text{ cm}^{-2} \text{ s}^{-1}$ and $P_{\nu_e \rightarrow \bar{\nu}_e} \leq 9.84 \times 10^{-5}$. For the high-energy window the sensitivities are $\phi_{\text{lim}} \leq 4.01 \times 10^1 \text{ cm}^{-2} \text{ s}^{-1}$ and $P_{\nu_e \rightarrow \bar{\nu}_e} \leq 2.07 \times 10^{-5}$ (the latter using $\Phi_{\text{SSM}}(E > E_{\text{th}})$). These results, summarized in Table 4, reflect the improved background conditions achieved above the visible-energy threshold.

Translating the (field-independent) probability sensitivities into magnetic-moment sensitivities with $\mu_{\nu} \propto \sqrt{P}/B_{\perp}$, we quote representative benchmarks. For tachocline-scale reference fields, $B_{\perp} = 50$ and 100 kG, we find $\mu_{\nu} \leq 1.58 \times 10^{-10} \mu_B$ and $7.91 \times 10^{-11} \mu_B$ (full window), and $\mu_{\nu} \leq 7.27 \times 10^{-11} \mu_B$ and $3.64 \times 10^{-11} \mu_B$ (high-energy window), respectively. For solar-interior benchmarks discussed in the text, $B_{\perp} = 600$ G and 7 MG, the analogous sensitivities are $\mu_{\nu} \leq 1.33 \times 10^{-8} \mu_B$ and $1.13 \times 10^{-12} \mu_B$ (full window), and $\mu_{\nu} \leq 6.07 \times 10^{-9} \mu_B$ and $5.18 \times 10^{-13} \mu_B$ (high-energy window). We emphasize that cross-experiment comparisons are made primarily in terms of the field-independent conversion probability; the mapping to μ_{ν} depends on the assumed B_{\perp} and is shown for illustrative benchmarks.

Placing these results in context with previous studies (Figure 1, Table 4) reveals a clear window dependence: in the 1.8–16.8 MeV region JUNO remains background-limited by near/far reactors and does not surpass the tightest existing limits; in contrast, in the 8.0–16.8 MeV window, where reactor contributions are strongly suppressed and the probability is normalized to $\Phi_{\text{SSM}}(E > E_{\text{th}})$, JUNO is competitive and slightly leading. Numerically, our projected probability sensitivity $P_{\text{lim}} \simeq 2.07 \times 10^{-5}$ improves upon the KamLAND 2022 result ($\sim 3.5 \times 10^{-5}$) by a factor ~ 1.7 , which corresponds to a modest $\sim 20\%$ tightening in μ_{ν} (given $\mu_{\nu} \propto \sqrt{P}$).

Overall, these findings highlight the scientific relevance of dedicated solar-antineutrino searches in large liquid-scintillator detectors. Because the near-reactor component is the dominant background at JUNO, continued refinement of the background prediction *both* together with optimized energy selections and, where possible, spectral-shape likelihoods will further enhance sensitivity to $\nu_e \rightarrow \bar{\nu}_e$ transitions and to μ_{ν} , advancing our understanding of neutrino electromagnetic properties and solar astrophysics.

REFERENCES

Abe, K., Bronner, C., Hayato, Y., et al. 2022a,
Astroparticle Physics, 139, 102702,
doi: [10.1016/j.astropartphys.2022.102702](https://doi.org/10.1016/j.astropartphys.2022.102702)

Abe, S., Asami, S., Gando, A., et al. 2022b, *ApJ*, 925, 14,
doi: [10.3847/1538-4357/ac32c1](https://doi.org/10.3847/1538-4357/ac32c1)

Abraho, T., Minakata, H., Nunokawa, H., & Quiroga, A. A. 2015, JHEP, 11, 001, doi: [10.1007/JHEP11\(2015\)001](https://doi.org/10.1007/JHEP11(2015)001)

Abusleme, A., Adam, T., Ahmad, S., et al. 2025, Chinese Physics C, 49, 033104, doi: [10.1088/1674-1137/ad7f3e](https://doi.org/10.1088/1674-1137/ad7f3e)

Aharmim, B., Ahmed, S. N., Beier, E. W., et al. 2004, PhRvD, 70, 093014, doi: [10.1103/PhysRevD.70.093014](https://doi.org/10.1103/PhysRevD.70.093014)

Akhmedov, E., & Pulido, J. 2003, Physics Letters B, 553, 7, doi: [https://doi.org/10.1016/S0370-2693\(02\)03182-9](https://doi.org/10.1016/S0370-2693(02)03182-9)

Aliani, P., Antonelli, V., Ferrari, R., Picariello, M., & Torrente-Lujan, E. 2003, PhRvD, 67, 013006, doi: [10.1103/physrevd.67.013006](https://doi.org/10.1103/physrevd.67.013006)

An, F., An, G., An, Q., et al. 2016, Journal of Physics G: Nuclear and Particle Physics, 43, 030401, doi: [10.1088/0954-3899/43/3/030401](https://doi.org/10.1088/0954-3899/43/3/030401)

Antia, H. 2008, Journal of Astrophysics and Astronomy, 29, 85, doi: [10.1007/s12036-008-0011-4](https://doi.org/10.1007/s12036-008-0011-4)

Bahcall, J. N., Fowler, W. A., Iben, Jr., I., & Sears, R. L. 1963, ApJ, 137, 344, doi: [10.1086/147513](https://doi.org/10.1086/147513)

Bahcall, J. N., Lisi, E., Alburger, D. E., et al. 1996, PhRvC, C54, 411, doi: [10.1103/PhysRevC.54.411](https://doi.org/10.1103/PhysRevC.54.411)

Bahcall, J. N., & Pinsonneault, M. H. 2004, PhRvL, 92, 121301, doi: [10.1103/PhysRevLett.92.121301](https://doi.org/10.1103/PhysRevLett.92.121301)

Balata, M., et al. 2006, Eur. Phys. J., C47, 21, doi: [10.1140/epjc/s2006-02560-4](https://doi.org/10.1140/epjc/s2006-02560-4)

Barger, V., Marfatia, D., Whisnant, K., & Wood, B. 2002, Physics Letters B, 537, 179, doi: [10.1016/s0370-2693\(02\)01955-x](https://doi.org/10.1016/s0370-2693(02)01955-x)

Beda, A., Brudanin, V., Egorov, V., et al. 2010, arXiv e-prints, doi: [10.48550/arXiv.1005.2736](https://doi.org/10.48550/arXiv.1005.2736)

Bellini, G., Benziger, J., Bonetti, S., et al. 2011, Physics Letters B, 696, 191, doi: <https://doi.org/10.1016/j.physletb.2010.12.030>

Capozzi, F., & Raffelt, G. 2020, Phys. Rev. D, 102, 083007, doi: [10.1103/PhysRevD.102.083007](https://doi.org/10.1103/PhysRevD.102.083007)

Carenza, P., Luente, G., Gerbino, M., Giannotti, M., & Lattanzi, M. 2024, PhRvD, 110, 023510, doi: [10.1103/physrevd.110.023510](https://doi.org/10.1103/physrevd.110.023510)

Cisneros, A. 1971, Ap&SS, 10, 87, doi: [10.1007/BF00654607](https://doi.org/10.1007/BF00654607)

de Holanda, P. C., & Smirnov, A. Y. 2002, PhRvD, 66, 113005, doi: [10.1103/physrevd.66.113005](https://doi.org/10.1103/physrevd.66.113005)

Eguchi, K., Enomoto, S., Furuno, K., et al. 2004, PhRvL, 92, 071301, doi: [10.1103/PhysRevLett.92.071301](https://doi.org/10.1103/PhysRevLett.92.071301)

Feldman, G. J., & Cousins, R. D. 1998, PhRvD, 57, 3873, doi: [10.1103/PhysRevD.57.3873](https://doi.org/10.1103/PhysRevD.57.3873)

Friedland, A. 2005, arXiv preprint hep-ph/0505165, doi: [10.48550/arXiv.hep-ph/0505165](https://doi.org/10.48550/arXiv.hep-ph/0505165)

Fukuda, Y., Hayakawa, T., Ichihara, E., et al. 1998, PhRvL, 81, 1562, doi: [10.1103/PhysRevLett.81.1562](https://doi.org/10.1103/PhysRevLett.81.1562)

Gando, A., Gando, Y., Ichimura, K., et al. 2011, PhRvD, 83, 052002, doi: [10.1103/PhysRevD.83.052002](https://doi.org/10.1103/PhysRevD.83.052002)

—. 2012, The Astrophysical Journal, 745, 193, doi: [10.1088/0004-637X/745/2/193](https://doi.org/10.1088/0004-637X/745/2/193)

Giunti, C., & Studenikin, A. 2009, Physics of Atomic Nuclei, 72, 2089, doi: [10.1134/s1063778809120126](https://doi.org/10.1134/s1063778809120126)

—. 2015, Rev. Mod. Phys., 87, 531, doi: [10.1103/RevModPhys.87.531](https://doi.org/10.1103/RevModPhys.87.531)

Heger, A., Friedland, A., Giannotti, M., & Cirigliano, V. 2009, The Astrophysical Journal, 696, 608, doi: [10.1088/0004-637X/696/1/608](https://doi.org/10.1088/0004-637X/696/1/608)

Huber, P. 2011, Phys. Rev. C, 84, 024617, doi: [10.1103/PhysRevC.85.029901](https://doi.org/10.1103/PhysRevC.85.029901)

Kitchatinov, L. 2008, Astron. Rep., 52, 247, doi: [10.1134/S1063772908030074](https://doi.org/10.1134/S1063772908030074)

Li, S.-P., & Xu, X.-J. 2023, Journal of High Energy Physics, 85, doi: [10.1007/JHEP02\(2023\)085](https://doi.org/10.1007/JHEP02(2023)085)

Lindner, M., Radovčić, B., & Welter, J. 2017, Journal of High Energy Physics, 2017, 1, doi: [10.1007/JHEP07\(2017\)139](https://doi.org/10.1007/JHEP07(2017)139)

Miranda, O., Rashba, T. I., Rez, A., & Valle, J. 2004, PhRvD, 70, 113002, doi: [10.1103/physrevd.70.113002](https://doi.org/10.1103/physrevd.70.113002)

Miranda, O. G. and Rashba, T. I. and Rez, A. I. and Valle, J. W. F. 2004, Phys. Rev. Lett., 93, doi: [10.1103/PhysRevLett.93.051304](https://doi.org/10.1103/PhysRevLett.93.051304)

Mueller, T. A., Lhuillier, D., Fallot, M., et al. 2011, Phys. Rev. C, 83, 054615, doi: [10.1103/PhysRevC.83.054615](https://doi.org/10.1103/PhysRevC.83.054615)

Particle Data Group. 2024, Prog. Theor. Exp. Phys., 2022, 083C01, doi: [10.1093/ptep/ptac097](https://doi.org/10.1093/ptep/ptac097)

Raffelt, G., & Weiss, A. 1992, A&A, 264, 536

Serenelli, A. M. 2010, Ap&SS, 328, 13, doi: [10.1007/s10509-009-0174-8](https://doi.org/10.1007/s10509-009-0174-8)

Stock, M. R. 2024, arXiv e-prints, doi: [10.48550/arXiv.2405.07321](https://doi.org/10.48550/arXiv.2405.07321)

Strumia, A., & Vissani, F. 2003, Physics Letters B, 564, 42, doi: [https://doi.org/10.1016/S0370-2693\(03\)00616-6](https://doi.org/10.1016/S0370-2693(03)00616-6)

Ventura, & Panibra, S. 2025, JUNO Event-Rate Calculator and Background Extrapolation Framework, v1.0, Zenodo, doi: [10.5281/zenodo.17613795](https://doi.org/10.5281/zenodo.17613795)

Vinyoles, N., Serenelli, A. M., Villante, F. L., et al. 2017, The Astrophysical Journal, 835, 202, doi: [10.3847/1538-4357/835/2/202](https://doi.org/10.3847/1538-4357/835/2/202)

Voloshin, M. B. 2010, PhRvL, 105, 201801, doi: [10.1103/PhysRevLett.105.201801](https://doi.org/10.1103/PhysRevLett.105.201801)

Wong, H. T., Li, H.-B., & Lin, S.-T. 2010, PhRvL, 105, 061801, doi: [10.1103/PhysRevLett.105.061801](https://doi.org/10.1103/PhysRevLett.105.061801)